



Article

Experimental Investigation on the Damage Evolution of Thermally Treated Granodiorite Subjected to Rapid Cooling with Liquid Nitrogen

Mohamed Elgharib Gomah ^{1,2}, Enyuan Wang ^{1,*} and Ahmed A. Omar ³

¹ School of Safety Engineering, China University of Mining and Technology, Xuzhou 221116, China; mohammedel-ghareeb.12@azhar.edu.eg

² Mining and Petroleum Engineering Department, Faculty of Engineering, Al-Azhar University, Cairo 11884, Egypt

³ Housing and Building National Research Center, Cairo 11511, Egypt; ahmed.abubakr@hbrc.edu.eg

* Correspondence: weytop@cumt.edu.cn

Abstract: In many thermal geotechnical applications, liquid nitrogen (LN₂) utilization leads to damage and cracks in the host rock. This phenomenon and associated microcracking are a hot topic that must be thoroughly researched. A series of physical and mechanical experiments were conducted on Egyptian granodiorite samples to investigate the effects of liquid nitrogen cooling on the preheated rock. Before quenching in LN₂, the granodiorite was gradually heated to 600 °C for two hours. Microscopical evolution was linked to macroscopic properties like porosity, mass, volume, density, P-wave velocity, uniaxial compressive strength, and elastic modulus. According to the experiment results, the thermal damage, crack density, porosity, and density reduction ratio increased gradually to 300 °C before severely degrading beyond this temperature. The uniaxial compressive strength declined marginally to 200 °C, then increased to 300 °C before monotonically decreasing as the temperature rose. On the other hand, at 200 °C, the elastic modulus and P-wave velocity started to decline significantly. Thus, 200 and 300 °C were noted in this study as two mutation temperatures in the evolution of granodiorite mechanical and physical properties, after which all parameters deteriorated. Moreover, LN₂ cooling causes more remarkable physical and mechanical modifications at the same target temperature than air cooling. Through a deeper comprehension of how rocks behave in high-temperature conditions, this research seeks to avoid and limit future geological risks while promoting sustainability and understanding the processes underlying rock failure.

Keywords: Egyptian granodiorite; liquid nitrogen; physical and mechanical properties; microscopical evolution; cooling impacts



Citation: Gomah, M.E.; Wang, E.; Omar, A.A. Experimental Investigation on the Damage Evolution of Thermally Treated Granodiorite Subjected to Rapid Cooling with Liquid Nitrogen. *Sustainability* **2024**, *16*, 6396. <https://doi.org/10.3390/su16156396>

Academic Editor: Jin Luo

Received: 25 June 2024

Revised: 15 July 2024

Accepted: 23 July 2024

Published: 26 July 2024

Correction Statement: This article has been republished with a minor change. The change does not affect the scientific content of the article and further details are available within the backmatter of the website version of this article.



Copyright: © 2024 by the authors. Licensee MDPI, Basel, Switzerland. This article is an open access article distributed under the terms and conditions of the Creative Commons Attribution (CC BY) license (<https://creativecommons.org/licenses/by/4.0/>).

1. Introduction

The increasing depletion of fossil fuels has led to an increased focus on the search for alternative energy sources, such as nuclear and geothermal energy extraction. Among the many renewable energy choices, these systems have been hailed as incredible, unexplored, and an environmentally viable replacement for traditional fossil fuels. For instance, geothermal energy is mainly stored within granite and is often found between 2 and 6 km below the surface at temperatures between 150 and 500 °C [1–4]. Over 255 trillion watt-hours of vast, unexplored, safe, and sustainable sources of green energy, which is nearly 300 times the heat of all fossil fuels combined, can be generated globally [5,6]. On the other hand, based on the already identified uranium reserves, today's commercial nuclear power plants powered by uranium can supply the world with clean, affordable, and dependable energy well into the next century [7,8]. Thus, many scholars have focused on understanding and assessing how high temperatures affect the behavior of rocks, which often deteriorate when the temperature exceeds the threshold [9–17].

The reservoir rocks in these systems are subjected to extreme heat stress [18–21]. The resulting thermal degradation can cause rock masses to become unstable and fail, ultimately resulting in catastrophic engineering events [22]. Therefore, understanding the evolution of thermally induced rock damage is crucial for disaster prevention in many geotechnical and energy engineering applications [8]. Moreover, the limited porosity, poor permeability, high density, and enormous buried depth of hot rock reservoirs make it challenging to exploit such high-temperature sources. Thus, establishing an efficient flow route in hot rock aquifers is one of the main issues in geothermal energy utilization [23]. Hence, hydraulic fracturing has significantly enhanced the exploitation efficiency of geothermal energy, oil/gas extraction, coalbed methane extraction, and nuclear energy during the last few years [24–29]. The results showed that thermal shock increases rock intrinsic cracks and reduces rock strength, improving HDR reservoir hydraulic fracturing performance [30–32]. Nevertheless, traditional hydraulic cracking is increasingly challenged due to formation destruction, environmental consequences, and water usage [33,34].

As an exceptionally low-temperature fluid [35], liquid nitrogen is projected to replace water-based cracking fluid to build fluid flow routes in low-permeability formations [36]. Enhanced permeability and increased rock-breaking effectiveness in geothermal reservoirs can be achieved using LN₂ [37]. Compared to conventional water/air cooling, applying LN₂ during the cryogenic fracturing procedure can create a significant thermal gradient and an abrupt temperature shift in the rock's inner and outer bodies, resulting in greater thermal stresses and more thermal cracks in rocks [38]. Liquid nitrogen quenching involves more intense heat transfer than air/water cooling. Therefore, the thermal cracking impact was significantly enhanced at high temperatures when the HDR reservoirs were stimulated by cryogenic LN₂. For instance, Zhang et al. [39] demonstrated that the crack networks produced by cryogenic fracturing improved HDR's capacity to extract heat. According to their findings, LN₂ fracturing technology holds great promise for the advancement of HDR. According to Yang et al. [40], cryogenic LN₂ stimulus enhanced the voids in the high temperatures of granite's fracture network and reportedly decreased failure stress. Moreover, when the temperature of the granite surpassed 200 °C, LN₂ stimulation offered outstanding benefits for HDR fracturing.

Changes in the mechanical and physical properties of heated rocks following LN₂ cooling were investigated by [41–43]. The findings indicate that while LN₂ cooling may provide a rapid cooling rate, the thermal damage to treated rocks following LN₂ cooling is greater than that following water and air cooling. Furthermore, LN₂ thermal shock damages rocks more severely at higher temperatures. Once LN₂ abruptly cools the hot rock within a short time, it experiences significant thermal stress that causes a "softening impact" [44]. Hence, major structural damage occurs during reservoir stimulation [41]. The principal contributions to rock degradation in the heating treatment are the loss of structural water and the growth of mineral particles [45]. However, thermal stress is the primary cause of rock damage throughout the cooling process, and the intensity of damage is related to the rate of cooling [3]. Wu et al. [46] discovered that when the temperature of the shale increased, LN₂ cooling caused an increase in rock damage. According to Huang et al. [47], the cryogenic impact on granite increased proportionately to the temperature differential between granite and LN₂. Using a series of studies, Wu et al. [48] looked into how heated granite changed mechanically and physically during LN₂ (cyclic) cooling. The outcomes showed that when LN₂ cooled granites at high temperatures, noticeable changes in their mechanical characteristics were seen. Cha et al. [49] developed a lab apparatus to conduct cryogenic LN₂ fracturing studies under triaxial loading conditions. Their results demonstrated that the thermal fissures caused by LN₂ treatment could lower the rock's breakdown stress.

Energy extraction operations are strongly associated with geological dangers resulting from cooling high-temperature rocks after contact with the stimulator. Hence, the effects of LN₂ cooling technology on thermally treated rocks have garnered much attention in recent years. As mentioned previously, studies have emphasized the benefits of using liquid

nitrogen cooling as a stimulant for fracturing. However, the cold environment damages and cracks the host rock during liquid nitrogen fracturing. This can damage rock pore systems and change their mechanical characteristics. Thus, it is also worthwhile to investigate how the physical and mechanical characteristics and fracturing features of high-temperature crystalline rocks vary when they are subjected to rapid LN₂ cooling shock. In addition, the LN₂ cooling technique has been applied to many rocks, such as granite, sandstone, marble, etc. Nevertheless, the feasibility and effectiveness of LN₂ cooling on many other rocks, such as Egyptian granodiorite, a widespread igneous rock in many applications, are still unclear. Hence, samples were subjected to various temperatures before being rapidly cooled using liquid nitrogen to study the thermal damage to granodiorite's physical and mechanical qualities. Understanding how the properties of granodiorite rocks begin to fail following heating/cooling treatment and how the microcracks spread is essential to promoting the sustainable development of geotechnical engineering. Therefore, by better understanding Egyptian granodiorite's behavior in hot conditions, such possible risks can be avoided or reduced.

2. Materials and Methods

Commonly, Neoproterozoic Egyptian granitoids are classified into the following two distinct varieties: older granite, which is dark gray and comprises tonalite to granodiorite, and young granite, which ranges in color from pink to red [50]. When silica-rich magma intrusion cools down in batholiths beneath the Earth's surface, plutonic igneous granodiorite is created. Granodiorite is a parasitical igneous rock that resembles granite in structure. It primarily includes plagioclase feldspar rather than orthoclase feldspar. Over 20% of granodiorite is quartz, and plagioclase makes up 65–90% of the feldspar, according to the Streckeisen Chart QAPF double triangle [51] (field 4). Because of a subequal mixing of light- and dark-colored minerals, the granodiorite under consideration has an equigranular texture, medium-to-coarse grain size, and a grayish-white color.

Granodiorite was collected from aged granite in the Eastern Desert of Egypt (close to Gabel Abu Marwa). The study location is situated 130 km southeast of Aswan, Egypt, between 23°00' and 23°10' northern latitudes and 33°17' and 33°28' east longitudes, as shown in Figure 1. For this study, granodiorite heated to high temperatures was drilled into 55.5 mm-diameter cylinders about 130 mm long, following the guidelines in ASTM D7012–14 [52]. Core specimens were extracted using a drilling apparatus. To prevent microcracking, a low coring rate was used during sample preparation, and the two ends were flattened to create flat, consistent surfaces. Finally, the specimens were kept at 105 °C for about 24 h (Nabertherm drying oven, made in Germany) to remove the moisture before testing.

At ambient temperature, the granodiorite samples had a Poisson's ratio of 0.19, an average uniaxial compressive strength (UCS) of 62.7 MPa, a Young's modulus of 48.2 GPa, a dry density of 2.7 g/cm³, and a P-wave velocity of 5752 m/s. As shown in Figure 2, X-ray diffraction analysis indicated that the rock composition was quartz, albite, hornblende, biotite, chlorite, etc.

Granodiorite specimens were divided into five groups, each subjected to the same thermal treatments to guarantee measurement accuracy. The reference set was maintained at ambient temperature without using the heating and cooling technique. Using an oven accuracy of ±3 °C in the "WiseTherm electric furnace FP/FHP (Figure 3a)", the samples were heated to the required temperatures of 200, 300, 400, and 600 °C, and the heating rate was set to 5 °C/min. After heating to the target temperature, the furnace was programmed to maintain a constant temperature for two hours to ensure uniform heating after reaching the target temperature for the whole sample. After that, LN₂ was used to rapidly cool the rock specimens after every heat treatment process (Figure 3b). After the heating and cooling procedure was completed, the specimens were dried. The variations in granodiorite's physical properties, such as porosity, water absorption, mass losses, volume enlargement, and density caused by the thermal treatments followed by the LN₂ cooling approach, were

determined. The portable ultrasonic nondestructive digital indicating tester (PUNDIT) was used to measure the P-wave velocity (V_p) of granodiorite samples before and after they were heated and cooled. Vaseline can improve the sensors and sample surface interaction and reduce reflection loss when the wave passes. Thus, it was frequently used as a coupler for V_p evaluation to produce suitably precise measurements. All the samples were divided into five groups, each involving three samples. Each specimen was subjected to five measures, and the average P-wave amount was selected as the P-wave velocity.

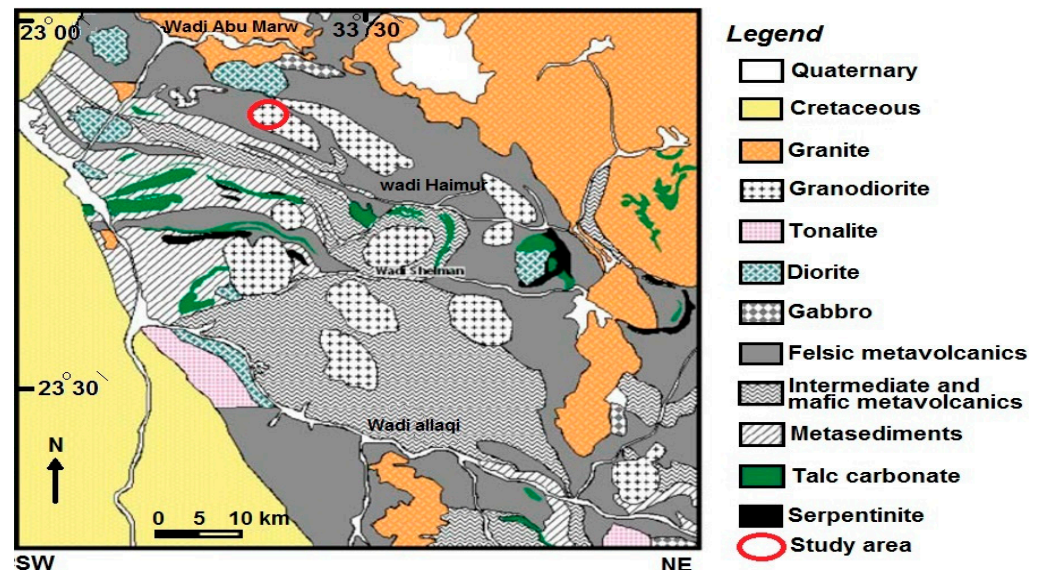


Figure 1. An Eastern Desert geological map of Egypt that includes the research area [53].

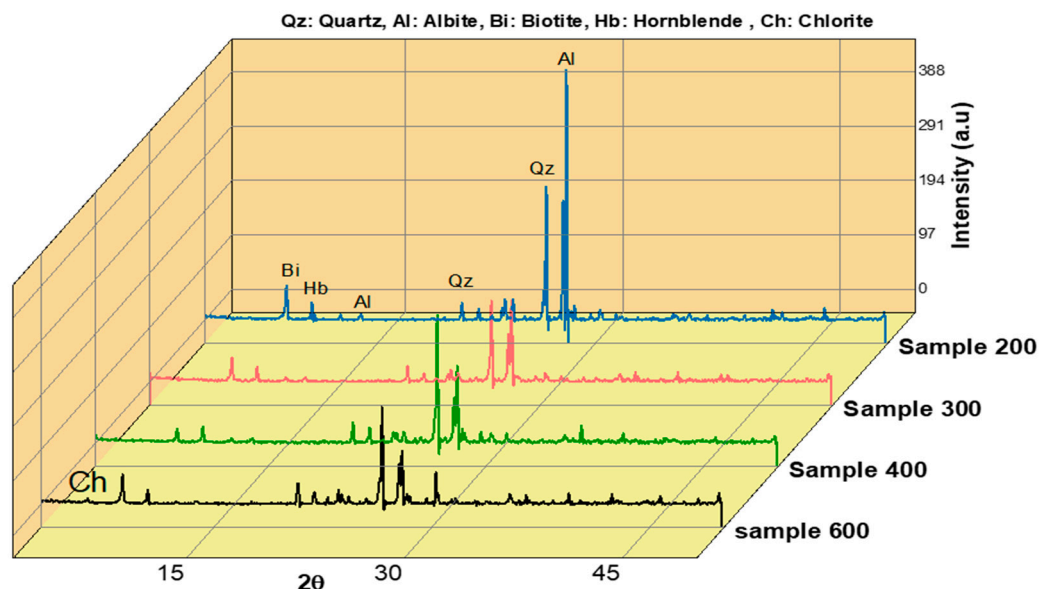


Figure 2. The XRD patterns of granodiorite samples at ambient temperature and following different treatments.

The typical granodiorite sample was ground to a fineness of about $75 \mu\text{m}$ for each group and then examined with an X-ray diffractometer, model X' Pert Pro Phillips MPD PW 3050/60. It has nickel-filtered $\text{Cu-K}\alpha$ radiation at 40 kv and 30 mA, scanning at a speed of $2\theta/\text{min}$, and a proportional digital counter. The radiation is available throughout a range of $0\text{--}50 2\theta$. To study the granodiorite microstructure, extra-treated, irregular samples were used. The treated samples, which were 0.5 cm long, representative cubic pieces,

were subjected to SEM analyses. Four thin slices of granodiorite were heated and cooled, and then they were looked at with the TESCAN VEGA3 instrument at magnifications from “400X to 1000X” to see their microscopic features (Figure 3c). This study used an Olympus BX50 transmitting polarizing microscope to analyze the microstructure of the granodiorite samples after they were heated and cooled in different ways (Figure 3d). For each prior treatment circumstance, a thin slice measuring 2.5 mm in length and roughly 0.03 mm in thickness was prepared. The rock sample’s microstructure was looked at with a magnification range of “4X to 40X” to see if any transgranular or grain boundary microcracks formed.

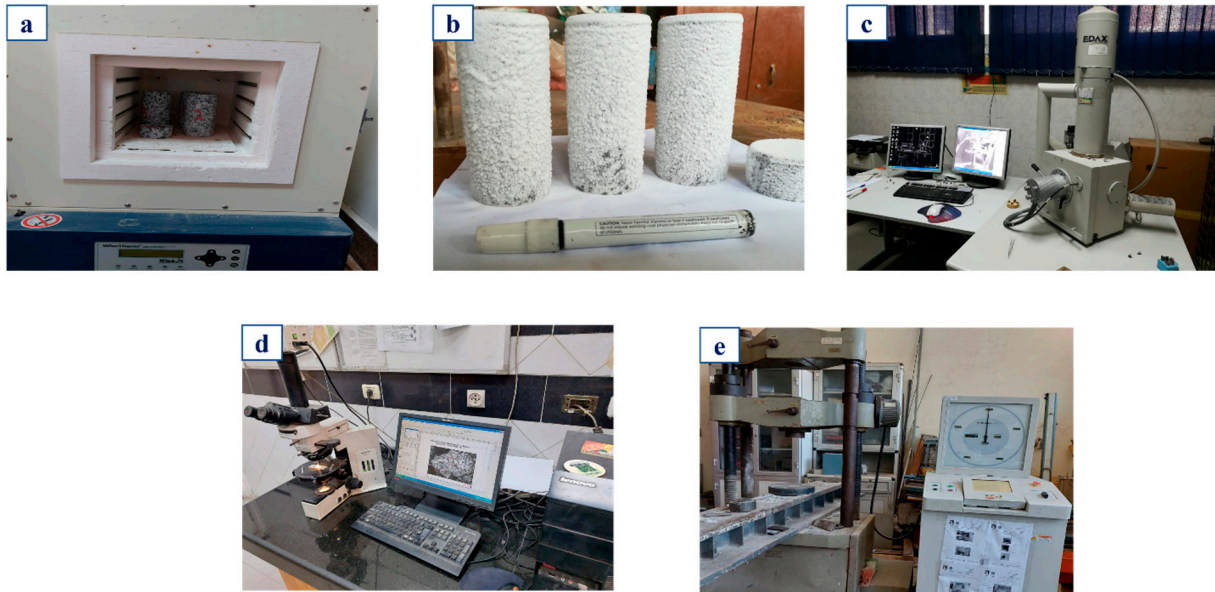


Figure 3. The principal devices used in this study: (a) the WiseTherm electric furnace, (b) quenched samples of liquid nitrogen, (c) the SEM apparatus, (d) the optical microscope device, and (e) a uniaxial compression test unit.

One of the key markers of the fundamental mechanical characteristics of rocks is the uniaxial compressive strength test. Using Shimadzu 500 KN RMU 57-2400 testing equipment, Japan (Figure 3e), a series of uniaxial compression tests were performed on granodiorite samples following the ASTM D7012-14 procedure. The equipment was connected to a data collection system, and two strain gauges and a linear variable differential transformer (LVDT) were used to find out how much the specimens moved in both directions while they were being loaded.

3. Results

3.1. Porosity and Absorption Deterioration

The physical property known as porosity plays a crucial role in governing rock’s physical and mechanical attributes, such as strength and deformation [54]. Thermal treatment considerably affects the porosity and, consequently, the water absorption capacity of the rock. Although at varying rates, the porosity and absorption capacity of the granodiorite specimens generally rose steadily with rising temperatures. Two phases of porosity and absorption modification with temperature are shown in Figure 4, before the mutation temperature point of 300 °C and after the mutation temperature point.

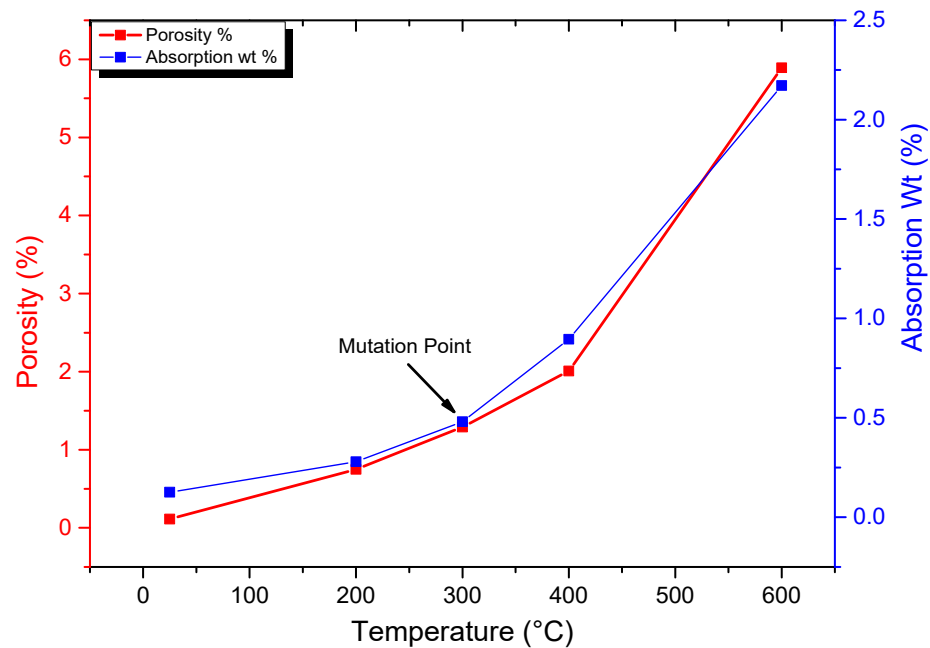


Figure 4. Porosity and water absorption responses of granodiorite samples following various thermal treatments and LN₂ cooling.

Under untreated conditions, the porosity of Egyptian granodiorite is 0.11%, which is the smallest. The porosity of granodiorite under LN₂ cooling treatment techniques rises with increasing heating temperatures. Granodiorite showed negligible variations in porosity and absorption during Phase 1 and up to 1.29% porosity and 0.48% absorption values at the mutation point of 300 °C. This indicated that very little “absorbed, interlayer, and mineral” water emerged from granodiorite during this phase. Once the temperature increases above 300 °C, the formation and propagation of thermal cracks brought on by thermal stresses are primarily responsible for the rapid increase in porosity after 300 °C, contributing to a massive growth in porosity (2.1%) and absorption (0.9%) at 400 °C. Some of the minerals disintegrate and break down at temperatures over 400 °C. Furthermore, at approximately 573 °C, α -quartz converts to β -quartz, resulting in considerable variations in porosity (5.9%) and absorption capacity (2.17%) at 600 °C.

3.2. Mass, Volume, and Density Behaviors

The mass-to-volume ratio is known as rock density. As the temperature rises, mass loss and volume expansion combine to cause a change in density. Figure 5 displays changes in density reduction rate “ $\eta\rho$ ” (blue curve), mass loss rate “ ηm ” (green curve), and volume growth rate “ ηv ” (red curve), with temperature change.

The figure shows that there is an increase in the mass loss rate, volume expansion rate, and density reduction rate when granodiorite experiences thermal heating and rapid quenching in LN₂. As illustrated in Figure 5, the granodiorite density loss rate gradually rises to the mutation point of 300 °C due to reduced mass loss and a small volume gain. After this temperature point, granodiorite mass, volume, and density changed rapidly. Mass, volume, and density changes were negligible up to 300 °C, coming in at 0.14%, 1.54%, and 1.65%, respectively. The rate of mass and density loss with volume expansion rate became apparent between 300 and 400 °C, and the values started to diverge. Hence, the values of ηm , ηv , and $\eta\rho$ were 0.33%, 5.48%, and 5.51%, respectively, at 400 °C. Volume growth and density drop rates were correlated when temperatures exceeded 400 °C and recorded a sharp rise, while an insignificant reduction in mass appeared. The values of volume and density were expanded at 600 °C, and values of 7.62% and 7.37% were recorded, respectively, as well as 0.34% for the mass loss rate. Thus, volume expansion is

a major factor in the decline in granodiorite density since, even at 600 °C, the specimens' mass loss rate is not much different from the original ones.

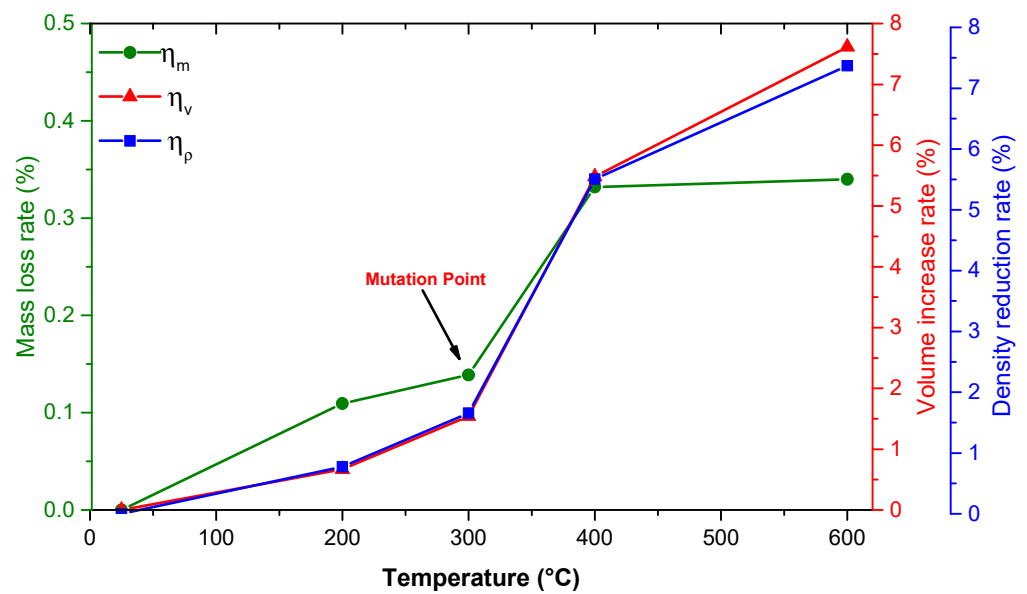


Figure 5. Mass loss, volume increase, and density reduction rates of granodiorite with target temperatures.

3.3. Ultrasonic Velocity

The P-wave velocity is a crucial metric that shows internal rock weaknesses. A lower V_P often denotes a higher frequency of local failures within rocks. Thus, P-wave velocity can be employed to assess the harm caused by heating and LN₂ cooling procedures. V_P decreases during heating and LN₂ cooling, as Figure 6 illustrates, and the variation rate increases as temperature rises.

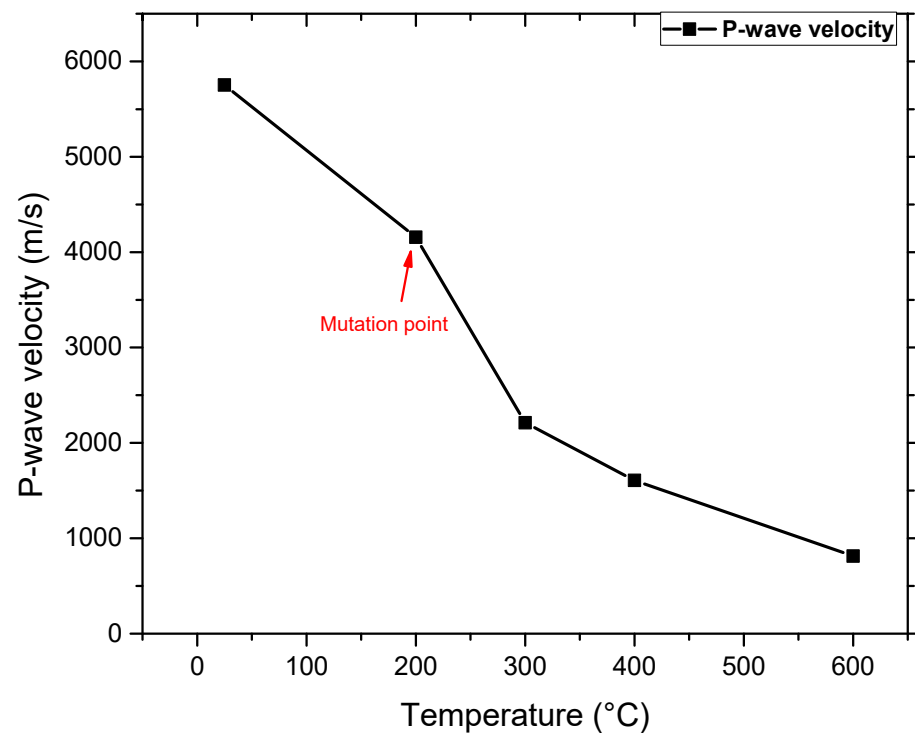


Figure 6. Change in P-wave velocity of granodiorite samples with temperature with LN₂ cooling treatments.

The V_P moderately dropped between room temperature and 200 °C. For instance, the P-wave velocity decreased from 5602 m/s at 25 °C to 4156 (with a 27% loss ratio). The P-wave reduction was noted after 200 °C, recording 2211 (62% loss ratio) at 300. As a result, 200 °C was selected as the P-wave velocity mutation point. Since sound waves move more slowly through the air than they do through rock, the P-wave velocity drops as a consequence. Also, the number of microcracks produced rises with the temperature and LN₂ quenching rate. Hence, a sharp decline in P-waves is observed after 200 °C, with the greatest reduction rate between 400 and 600 °C (Figure 6), including a 72% reduction ratio at 400 °C and an average P-wave reading of 813 m/s with an 86% reduction ratio at 600 °C.

3.4. SEM Observation

The microstructure of the investigated samples shows the development of thermal cracking, which results from heating, followed by cooling. The thermal expansion coefficient for each mineral in the investigated rock is important in developing thermal microcracks within the microstructure. Figure 7 depicts the alterations in the microstructural attributes of the granodiorite after applying heating and LN₂ cooling procedures. The granodiorite was subjected to temperatures of 200, 300, 400, and 600 °C during the heating process. In the presence of LN₂ cooling, observable intercrystalline thermal cracks and inevitable transcrystalline cracks are evident. The microcracks initiate the development of weak planes within the crystals. Some minerals can crack along preferred planar, such as cleavages, in response to external distribution [55]. According to SEM observations, very few cracks (boundary “bc” and transgranular “tc”) were discovered, and most cracks were dispersed and unconnected once the temperature was 200 °C (Figure 7a).

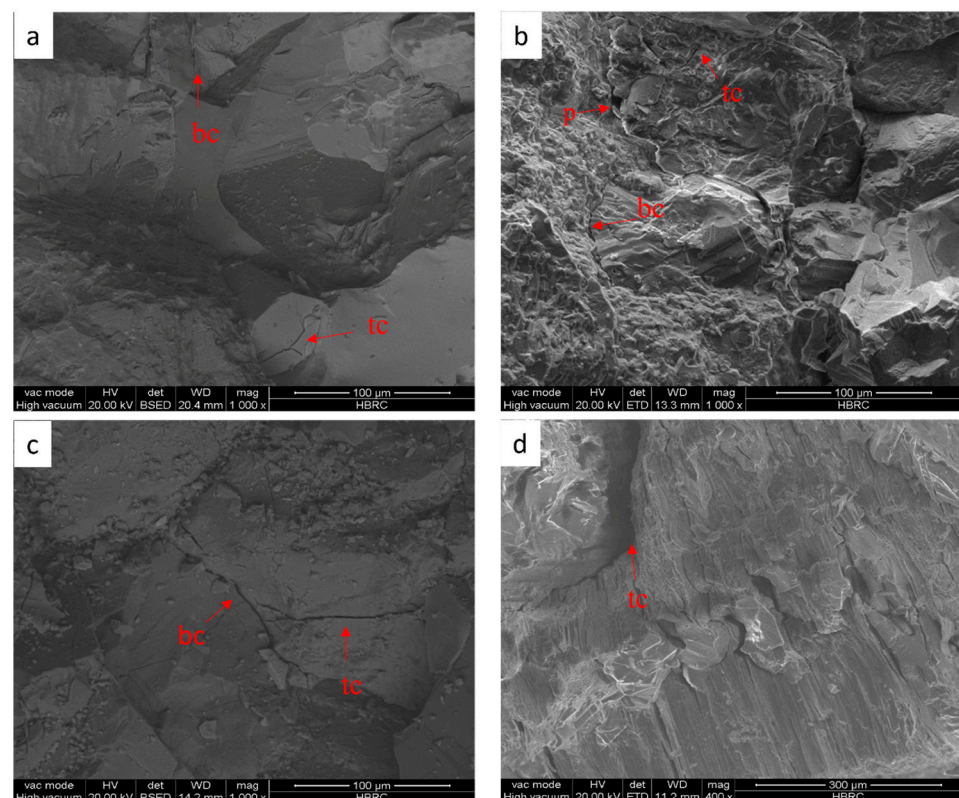


Figure 7. SEM images of granodiorite thermally treated and quickly cooled via LN₂ at 200 °C (a), 300 °C (b), 400 °C (c), and 600 °C (d). (bc) is boundary microcracks, and (tc) is transgranular microcracks.

The granodiorite that was heat-treated remained intact. Thermal cracking rose in the rock when the heating temperature was above 200 °C. Thus, the frequency and width of microcracks greatly increased once the granodiorite was thermally heated to 300 °C

(Figure 7b). The granodiorite's crystal surface became rough, and boundary and trans-granular fissures started to join and expand when the temperature approached 400 °C (Figure 7c). Tiny detachments were observed on the particle edges. Specimen integrity was compromised for the 600 °C specimens, and locally crushed zones were developed (Figure 7d). Moreover, as illustrated in Figure 8, many heat microcracks were driven to connect and merge, which made the macroscopic fracture density and crack length much bigger.

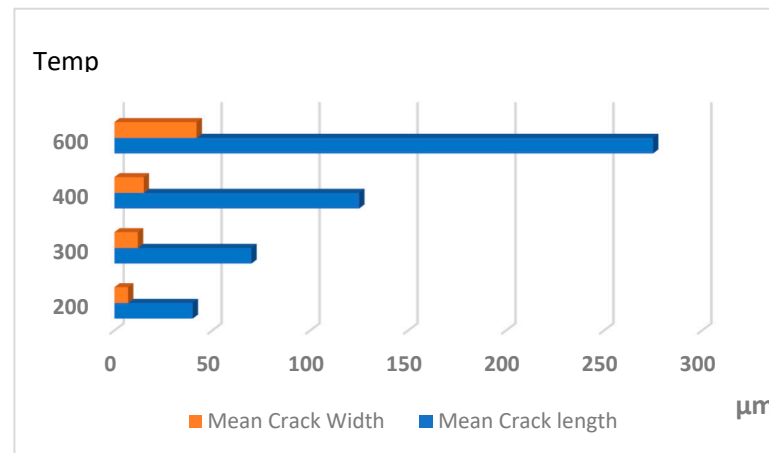


Figure 8. Crack length and width evolution of granodiorite specimens subjected to various thermal treatments and LN₂ rapid cooling.

Moreover, Figure 9 shows a diagram for microstructure changes resulting from heat treatment, followed by rapid cooling using LN₂. At 200 °C, the heat treatment causes the evaporation of free water within the microstructure, producing some tiny pores. In addition, a few discontinuous microcracks appear to propagate from particle edges. By increasing the temperature to 300 °C, the effect of thermal expansion and cooling shrinkage is reflected on the microcracks, and the percentage, length, and width of cracks increase within the microstructure. At 400 °C, roughness was observed on the surface of the grains, as well as the detachments of tiny particles. Continuous microcracks and large fractures penetrate the microstructure, and pores were observed when the temperature reached 600 °C.

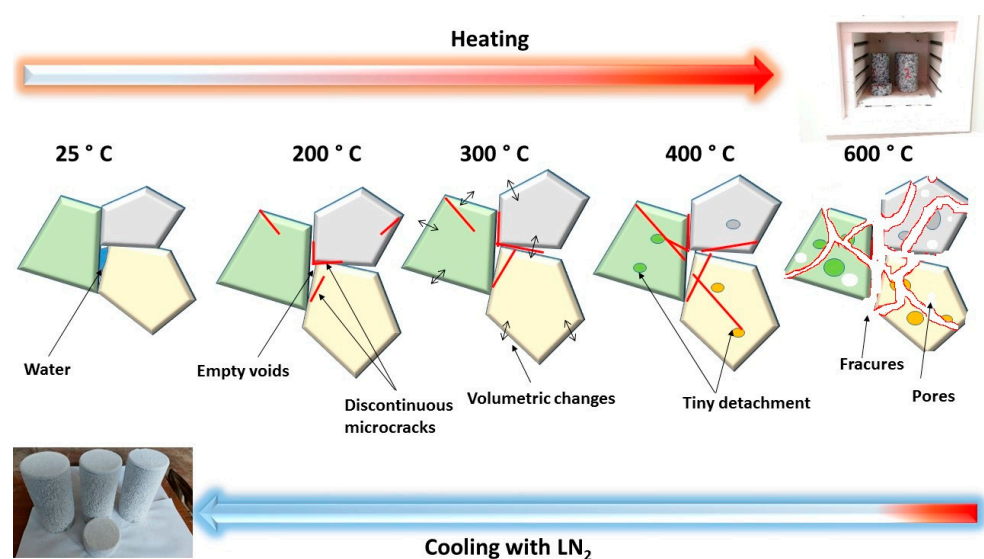


Figure 9. Diagram of the microstructural changes in studied samples after heat treatment, followed by rapid cooling using LN₂.

3.5. Mechanical Properties

3.5.1. UCS

Temperature-related changes to the microstructure and thermal expansion of minerals cause most of the mechanical characteristics of rock to deteriorate. From room temperature to 600 °C, the UCS of granodiorite samples that had been thermally treated and quickly cooled with LN₂ was assessed (Figure 10). UCS first slightly decreased to 200 °C after LN₂ cooling from 62.7 MPa at room temperature to 62.2 MPa at 200 and subsequently rapidly increased to 80 MP at 300 °C. As the temperature increased steadily, the granodiorite matrix's compaction and integrity deteriorated, sharply expanding the rock's compressibility and reducing its macroscopic strength. A notable UCS drop happens when the heating temperature increases over 300 °C due to the rise of microcracks, micro-defects, and empty spaces brought on by water evaporation. Consequently, following LN₂ cooling treatments, the granodiorite's UCS decreased significantly from 80 to 40 MPa, which is a 50% loss at temperatures between 300 and 400 °C.

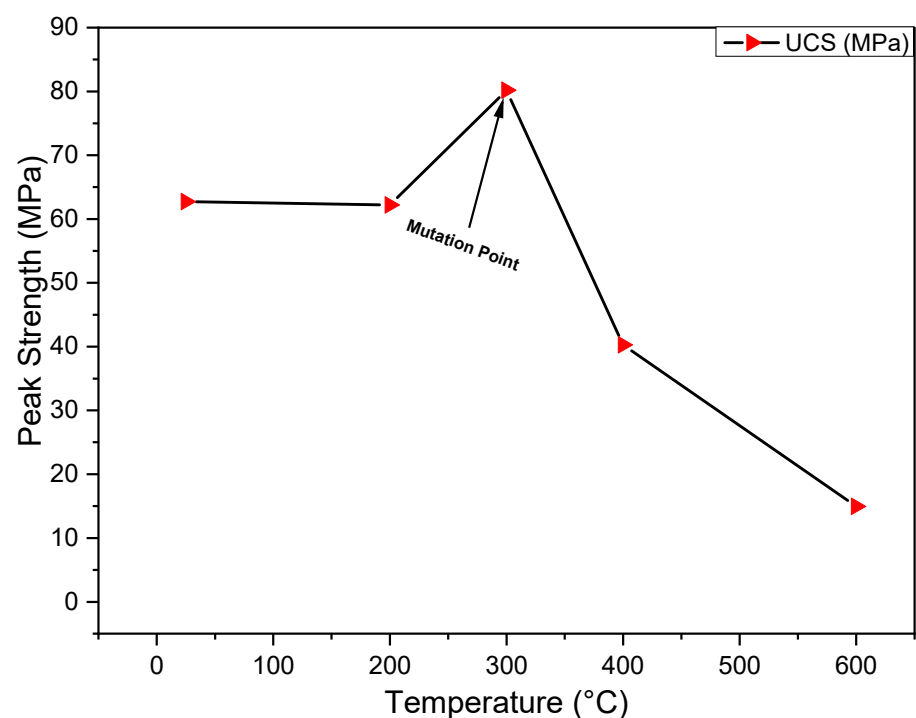


Figure 10. The change in the uniaxial compressive strength (UCS) of granodiorite after heat treatment and LN₂ cooling.

When the temperature rose beyond 400 °C, the combined effects of applied uniaxial compression and thermal stress led to the extensive formation of new microcracks, which ultimately caused the granodiorite specimen to shatter. Furthermore, the quartz alpha-beta transition caused a further drastic decrease at roughly 573 °C. According to this, the mutation temperature for granodiorite microstructural and UCS shifts is 300 °C. The compressive strength of the granodiorite dropped considerably from 40 to 15 MPa at 400–600 °C. Therefore, LN₂ cooling can significantly reduce the uniaxial compressive strength of granodiorite.

3.5.2. E

The impact of various temperatures followed by rapid cooling by LN₂ on Young's modulus was explored in this section since it is a vital metric in assessing mechanical deterioration. Figure 11 displays the elastic modulus values of the heated granodiorite samples at different temperatures under liquid nitrogen cooling conditions. For the samples under study, variations in the elastic modulus were not significant at 200 °C. As seen in

Figure 11, the cooling strategy had no clear adverse impacts, and a slight decline in the elastic modulus from 48 to 44.4 GPa in this temperature range was recorded.

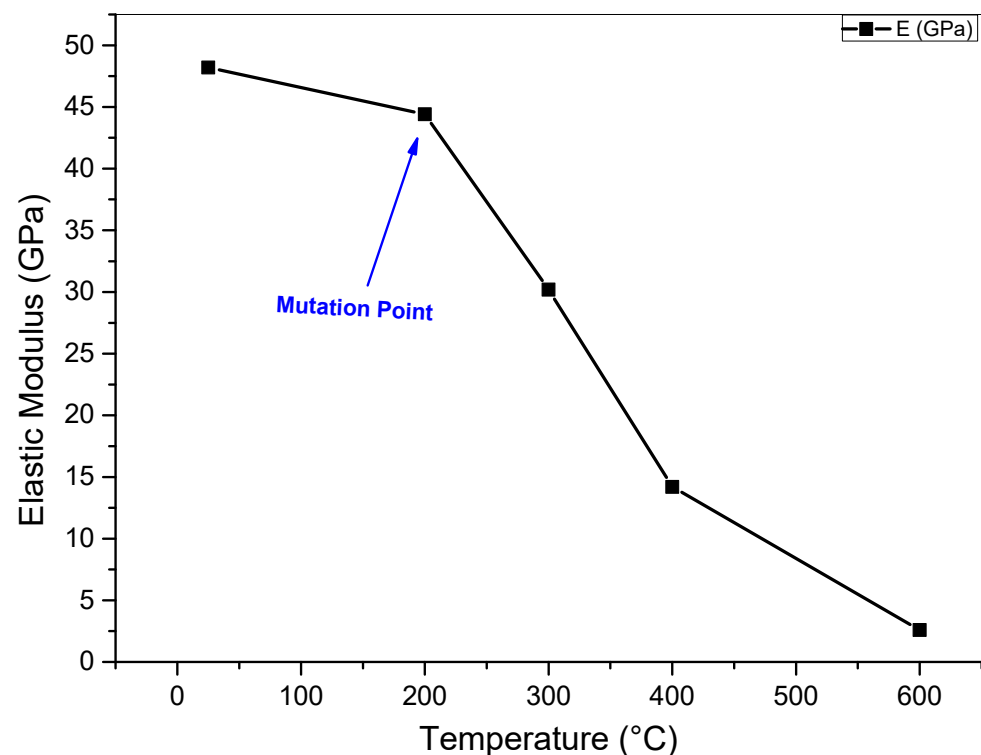






Figure 11. The elastic modulus (E) of granodiorite as a function of temperature and LN₂ cooling approach.

Due to the combined impacts of thermal stress and LN₂ cooling, the granodiorite degraded at a temperature above 200 °C, considerably boosting the production of new microcracks. Consequently, the granodiorite's elastic modulus dropped dramatically from 44.4 to 14.2 GPa at temperatures between 200 and 400 °C, indicating that 200 °C is the mutation temperature point for granodiorite elastic modulus shifts. After 400 °C, the cohesiveness of the mineral particles was weakened by these higher temperature ranges, which resulted in thermal softening and microstructural deterioration throughout the rock, which in turn, caused a significant drop in the elastic modulus. Thus, the elastic modulus dropped enormously from 14.2 GPa to 2.6 GPa between 400 and 600 °C.

3.5.3. Failure Modes

The final reflection of microcracks, beginning with development, and coalescence until the creation of macrocracks is the failure mode of rocks, which is crucial information for understanding the damage mechanism. The failure modes of the thermally treated granodiorite samples at different temperatures immediately quenched in LN₂ following the compression stress were compared and studied. Table 1 displays the failure mechanisms for the preheated granodiorite specimens at 200, 300, 400, and 600 °C. The findings show that samples typically fail at lower temperatures (200 °C) by axial splitting, whereas shear failure develops at higher temperatures (above 200 °C). Hence, strong external stimuli like LN₂ thermal shock will affect the granodiorite's micro- and macro-scale failure properties.

Table 1. Failure modes of granodiorite specimens subjected to LN₂ rapid cooling after different thermal treatments.

Temperature	200 °C	300 °C	400 °C	600 °C
Failure Mode				

The granodiorite has fewer fractures and a failure plane that is typically parallel to the loading axis at temperatures of 200 °C. In contrast, the thermal treatments and LN₂ cold shock led internal cracks to develop at heating temperatures of 300, 400, and 600 °C, which resulted in thermal cracks impacting the failure plane that was not completely parallel to the loading direction. Hence, all the rock samples' failure modes were shears, and they were typically present in combination with some severe failure and spreading fractures at 600 °C.

4. Discussion

Discussion is held over how cooling with LN₂ affects the preheated granodiorite's physical and mechanical properties and the start and spread of fractures. Hence, this section links the alterations in the responses of granodiorite properties with the registered microstructural changes, as concluded in Figure 12. Moreover, it examines the characteristics and mechanisms of heat-induced damage followed by rapid quenching.

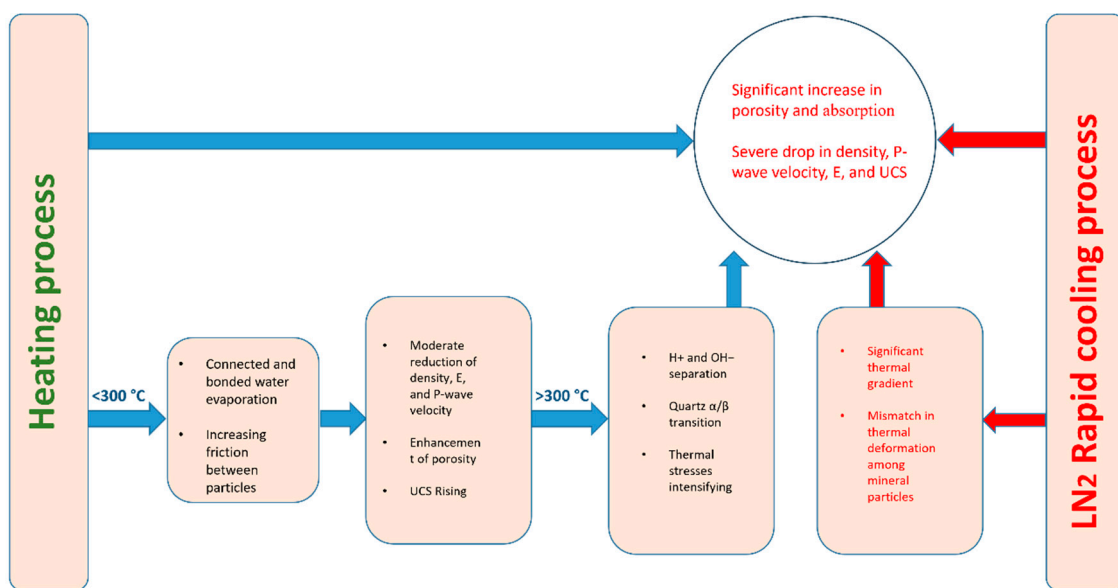


Figure 12. Physical and mechanical property responses during heating and LN₂ cooling processes.

4.1. Microstructural Evaluation

In addition to SEM investigations, the current study used an optical microscope to look at how different temperatures, followed by a cooling shock technique using LN₂, affected the evolution of cracks in granodiorite specimens. Biotite (Bi), albite (Al), hornblende (Hb), and quartz (Qz) were the main types of grains found in granodiorite samples. These grains were moderate to coarse (Figures 13 and 14). The mismatch in thermo-physical properties among various mineral particles significantly impacts the occurrence of thermal shock in rocks, which causes rock damage [36]. The application of LN₂ cooling induces damage to internal structures due to the discrepancy deformation of neighboring mineral grains, which can be attributed to variations in their respective thermal expansion coefficients. Consequently, this phenomenon leads to the creation of boundary fissures within the granodiorite. The magnitude of the coefficient of thermal expansion is intimately associated with the crystallographic orientations of the same mineral. Hence, transgranular cracks can be readily formed because of the disparity in deformations occurring along distinct crystallographic orientations. As seen in Figure 13a,b, optical microscopic observations reveal that boundary and transgranular cracks primarily disperse at the edges and within quartz minerals up to 300 °C.

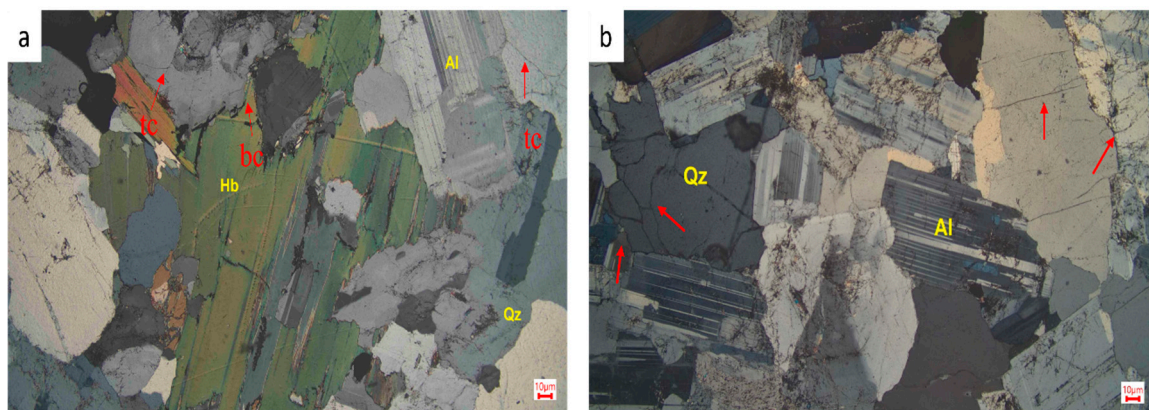


Figure 13. Crack evolution in granodiorite specimens subjected to different thermal treatments (a) at 200 °C and (b) at 300 °C and rapid cooling with LN₂, as seen using an optical microscope.

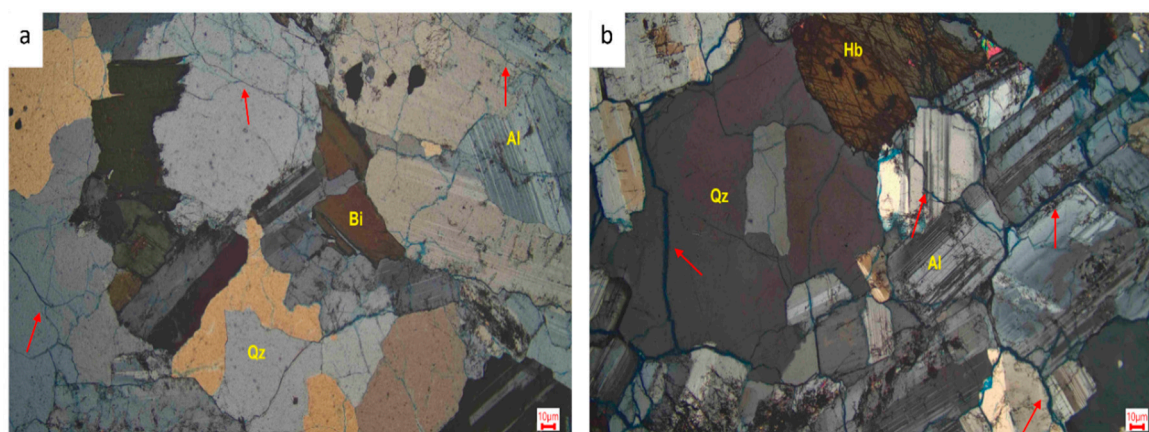


Figure 14. Crack evolution in granodiorite specimens subjected to different thermal treatments (a) at 400 °C and (b) at 600 °C and rapid cooling with LN₂, as seen using an optical microscope.

The high thermal expansion coefficient of quartz minerals may be related to this phenomenon. There may be significant mismatched deformations at the quartz borders and, consequently, high local thermal stresses because of the stark differences in the thermal expansion coefficient among quartz and other nearby minerals. The sharp shock from

the LN₂, combined with the increased temperature-induced thermal stresses, led to the initial cracks propagating and growing larger, significantly weakening the rocks' structural integrity. As seen in Figure 14a, the crack density of granodiorite was, therefore, much more significant at 400 °C than at 300 °C. Extensive boundary and transgranular cracks, resulting from increased internal stresses from the mineral-to-mineral thermal expansion mismatch, become visible when the temperature reaches 600 °C (Figure 14b). On the other hand, quartz is of the α -type at ambient temperature, and it experiences an expansion of roughly 0.45%, along with a shift in crystal structure to the β -type at 573 °C [56].

Microstructure changes generated by the α - β -type transitions in crystal structure lead to a notable rise in microcrack density and the creation of microcracks [57]. Once the temperature increases to 600 °C, large transgranular cracks are seen in the SEM image (Figure 7d). Hence, the boundary and transgranular cracks produced at 600 °C are substantially greater than those formed at 400 °C. The thermally treated granodiorite exhibits many transgranular cracks, although boundary cracking remains the main failure route at 600 °C. As seen in Figure 14a,b, it is observed that most of the freshly created transgranular cracks form in all granodiorite minerals. Moreover, the α - β -type transformation of quartz can be directly linked to the notable increase in porosity beyond 500 °C. The LN₂ cooling rate significantly impacts the formation of microcracks in granodiorite and, subsequently, the porosity alteration. Hence, in the current study, porosity was increased from 0.11% (in the initial condition) to 5.9% (heated to 600 °C). This is higher than what was seen in [58], in which porosity increased from 0.54% (in the initial state) to 4.25% (600 °C).

4.2. Physical Property Responses

According to this study, the physical properties of granodiorite that were thermally heated and rapidly cooled by LN₂ can be divided into the following two stages: before the mutation temperature point of 300 °C and after the mutation temperature. Because of thermal stress, the high-temperature treatment modifies the physical parameters of the rocks and causes new microcracks and microstructural deterioration within them. Hence, the initial rock cracks, mineral makeup, and water content will also all change following the LN₂ thermal shock, which will alter the properties of rocks. The primary cause of granodiorite porosity fluctuation when the temperature is below the threshold value is the loss of different kinds of water. Thus, the presence of water significantly impacts the porosity and absorption capacity. At temperatures between 100 and 250 °C, absorbed and interlayer water will evaporate, and structural water evaporates at temperatures above 300 °C [59]. The photomicrograph of the thermally treated granodiorite samples up to 300 °C (Figure 7a,b) clearly shows that a small number of microcracks began to form, which indicates the porosity and absorption showed moderate values (Figure 4). Consequently, the causes of porosity fluctuation up to 300 °C include mineralogical water and heat-induced vaporization.

Once heat treatment increases, some granodiorite minerals break down, while clay minerals dehydrate and completely lose structural water, which could lead to a rise in porosity and fracturing. In the heating process, the internal and external parts of the samples are subjected to tension and compression stresses, respectively. As a result, granodiorite is weathered by alternating thermal strains during the heating and LN₂ cooling procedures. As the heating temperature rises, fatigue failures induced by alternate loads develop, resulting in more local microcracks in rocks [46]. This clarifies how granodiorite's porosity increases with temperature. Therefore, the region between 300 and 400 °C, on the other hand, is distinguished by a rapid rise in porosity and absorption. Thermal stresses are the main reason for the sharp increase in this zone as thermal cracks develop and expand. After 400 °C, minerals like biotite, feldspar, and quartz experience varied internal stresses when heated due to their varying thermal expansion coefficients [60]. The growth of microcracks gradually raises the microcrack density due to these recently formed stresses. Additionally, significant alterations in porosity and absorption are caused by the breakdown of minerals and the α - β quartz phase transition.

On the other hand, the thermal treatment of rock results in several changes, including changes to the sample mass, size, and form, which affect the specimen's bulk density and volume. Granodiorite sample mass, volume, and hence, density were assessed before and after thermal treatment (heating and LN₂ quick cooling). Granodiorite mass falls following thermal loading, as Figure 5 illustrates. The main reason that granodiorite loses weight is because various kinds of water evaporate [45]. The rate at which granodiorite mass drops with temperature is sluggish because of the small amount of water content before 300 °C. In contrast, thermal stresses induce minerals and microcracks to expand thermally at high temperatures, which in turn, causes rocks to lose density due to volume expansion. Therefore, volume growth significantly decreases granodiorite density even 300 °C since the masses of the specimens differ little from the ones that were not treated. However, structural water quantities dropped due to dehydroxylation, and crystalline water amounts dramatically decreased due to mineral dehydration above 300 °C. The result was a sharp increase in the mass loss rate, which suggested that the internal minerals of the granodiorite samples had undergone substantial chemical and physical changes. Moreover, thermal treatment and rapid cooling cause alternating thermal stresses in rock, which break down the cementation between minerals and cause numerous microcracks in granodiorite samples because of the mismatch in thermal deformation among nearby mineral particles. Hence, the microcracks were expanded, increasing the granodiorite samples' total volume expansion rate. The physical characteristics changed from a stable to an unstable condition between 300 and 400 °C after the mutation point, and high values for the volume rise ratios produced a remarkable effect on the density reduction ratio. The difference in the thermal expansion of the minerals approaches its maximum after 400 °C. Thus, at 600 °C, granodiorite undergoes significant thermal degradation, which causes a massive increase in density loss and volume expansion rates. In line with earlier studies utilizing different cooling approaches [61,62], the reduction rate of density for the LN₂ cooling technique is identical to the detected modification in volume growth rate. Hence, at 600 °C, significant associated variations in density are because of volume expansion and are mainly caused by the quartz shift at 573 °C.

Granodiorite ultrasonic velocity significantly drops as the temperature rises (Figure 6). This resulted from thermal cracking, which also caused the separation of cleavage planes within the grains and the growth and propagation of internal cracks and voids, which often occur along the boundaries of grains. Furthermore, as temperature increases, the P-wave velocity falls; with LN₂ cooling, this decreasing trend accelerates compared with the other cooling methods studied by [62]. This proposes that as the temperature grows, the granodiorite treated with LN₂ cooling has more macropores and microfractures, which increase the porosity and the absorption of P-wave velocity (Figure 15). As a result, the internal microcrack surface experiences increased friction and slippage, significantly increasing the energy percentage loss.

SEM and OM observations show that as temperatures rise, the number of microcracks inside granodiorite increases, which causes a significant decrease in P-wave velocity. Before 200 °C and beyond 200 °C are the two stages of the speed vs. temperature curve. Between RT and 200 °C, wave velocity steadily decreased. The number of voids caused by the evaporation of different kinds of water (absorbed, interlayer, and mineral) was the primary cause of the V_p drop. Several microcracks appeared as the temperature rose above 200 °C, and the average P-wave rate severely declined as the temperature increased. The primary cause of this is the difference in the thermal expansion coefficients of granodiorite minerals, which leads to the formation of new fractures and the propagation of existing ones. In addition, variations in the mineral's thermal expansion along various crystallographic axes after 400 °C led to structural damage when heated, compromising the structural integrity of the rock. Hence, the measured V_p loss ratio peaked at 600 °C because of the high temperature and quick quenching by LN₂, significantly damaging the microstructure. Moreover, the P-wave demonstrated that the granodiorite structure was affected by the

LN₂ cooling method following thermal treatments, compared with other cooling processes in the aforementioned studies [63].

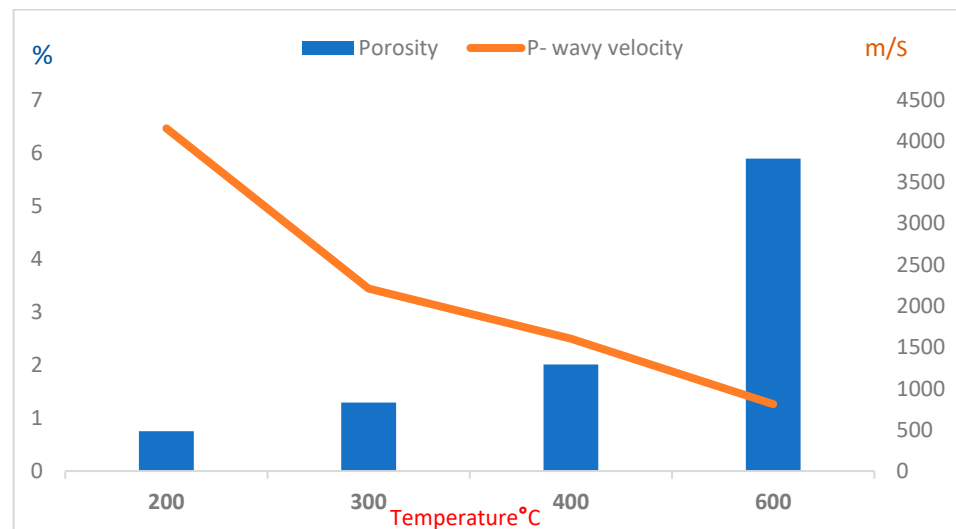


Figure 15. Relation between P-wave velocity and porosity of thermally heated granodiorite, followed by the LN₂ cooling method.

4.3. Mechanical Properties Responses

Granodiorite is a heterogeneous rock that includes various minerals with different thermal expansions of its minerals. Consequently, the mechanical characteristics of granodiorite will be affected mainly by temperature, and unpredictable thermal fractures will occur once thermal stress between or inside minerals exceeds their maximum strength [64]. Microcracks play both roles in the mechanical properties of the studied rocks, causing thermal degradation and hardening, according to UCS data [65]. Since thermal degradation has happened below 200 °C, the looseness of the mixture with rock minerals and the scaping of the interlayer water in the small holes and the connected water cause a modest decline in both the UCS and the elastic modulus of granodiorite [45].

On the other hand, thermal treatment can increase rock strength by inducing plastic expansions in minerals and increasing friction between minerals at a specific temperature limit. As a result, at 300 °C, the temperature enhanced the strength of the rock by causing the minerals to expand plastically and increasing friction between the particles (Figure 12). So, the granodiorite peak stress increased gradually, going from 62 MPa at 200 °C to 80 MPa at 300 °C. However, the elastic modulus still moderately declines in this temperature range. There was a significant 50% reduction in the granodiorite's UCS, from 80 to 40 MPa, at temperatures between 300 and 400 °C. The elastic modulus, too, dropped dramatically from 30 to 14 GPa. The granodiorite matrix became softer and lost integrity, significantly increasing the rock's compressibility and decreasing its macroscopic strength. This is brought on by the diffusion of tiny fractures, flaws, and empty spaces left behind by evaporating water. Hence, the unconfined compressive strength and elastic modulus values decreased throughout the uniaxial compressive strength experiments. The granodiorite samples began to degrade severely at temperatures above 400 °C, significantly accelerating the creation of new microcracks due to the combined impacts of rapid quenching by LN₂ and thermal stress. In addition, the transition between quartz's alpha and beta phases resulted in a significant decrease in this temperature limit, at roughly 573 °C. Thus, the granodiorite's elastic modulus drastically dropped from 14 to 2.6 GPa, and its compressive strength sharply fell from 40 to 15 MPa at 400 to 600 °C.

4.4. Thermal Damage Evolution of V_p and E

In geotechnical engineering, thermal damage mechanics has recently become a cutting-edge method for researching rock thermodynamics. The differences in thermal damage reflect changes created in the rock's microstructure by the cooling technique. The degree of thermal damage characteristic of rock can be predicted using many factors. This study used the P-wave velocity and the elastic modulus to figure out the thermal damage factor of granodiorite and to find out how that factor affected the rock's internal structure [66]. Equations (1) and (2) show that the ratio of the factor at the selected temperature to the value at room temperature is known as the thermal damage factor D and can be described as follows:

$$D(E) = 1 - \frac{E_T}{E_0} \quad (1)$$

$$D(v_p) = 1 - (V_{p_T}/V_{p_0})^2 \quad (2)$$

where (D) is the thermal damage factor, and the variables in the formula with the subscripts 0 and T are data obtained from granodiorite samples at room and target temperatures, respectively. The relationship between the granodiorite's thermal damage factor for P-wave velocity and elastic modulus with applied temperatures and the LN₂ cooling method is depicted in Figure 16.

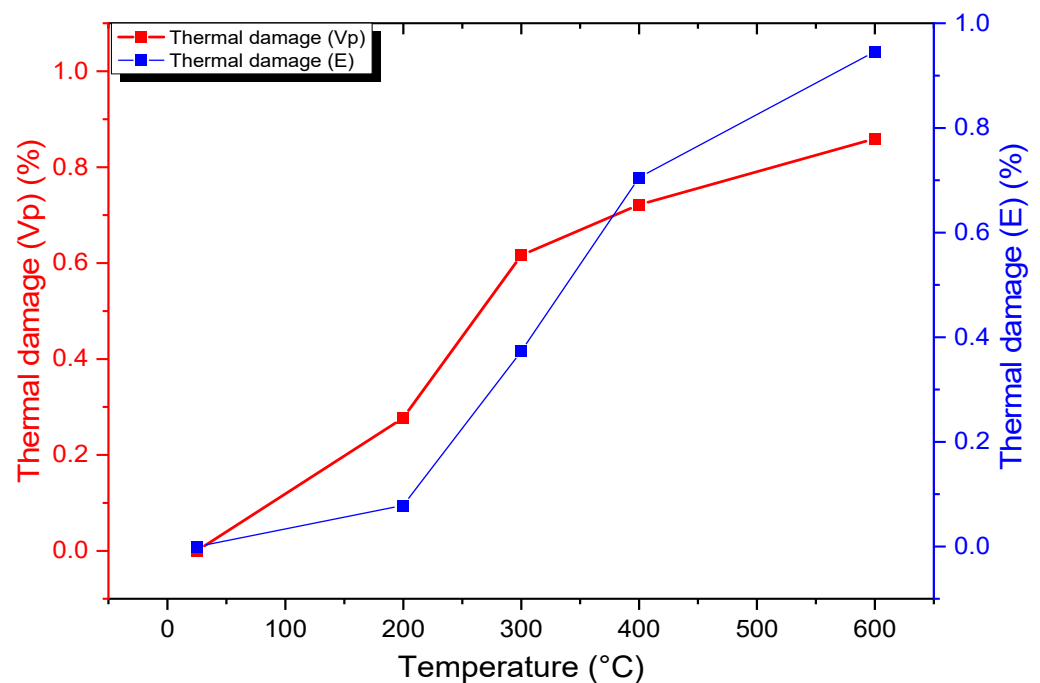


Figure 16. Thermal damage evolution of P-wave velocity and elastic modulus of thermally heated granodiorite, followed by the LN₂ cooling approach.

As demonstrated in Figure 16, there is a direct relationship between the degree of thermal damage and the heating/LN₂ cooling technique. Thermally treated granodiorite's thermal damage factor with LN₂ cooling increased with the various heating temperatures and showed a similar pattern for $D(V_p)$ and $D(E)$. The rock's deformation zone under external loads is reduced when pores and fissures close. Thus, even in heat damage, the elastic modulus varies minimally, and the resistance to deformation does not significantly deteriorate. Hence, there was a slight variation in the thermal damage factor, with 8% for the elastic modulus. In comparison, a moderate rise of 27% in P-wave velocity occurred when the granodiorite heating temperature was below 200 °C. However, the thermal damage in the studied parameters increased sharply when the heating temperature surpassed 200 °C. Moreover, the P-wave velocities became more temperature-sensitive than the elastic

modulus up to 300 °C. Consequently, the D (V_p) of the granodiorite samples was higher than the D (E), even though E was more vulnerable to thermal degradation below this point. Therefore, these findings suggest that the P-wave velocity and elastic modulus are sensitive and appropriate parameters for characterizing the thermal shock damage to granodiorite. Raising the heating temperature alters some minerals' framework structures and intensifies the thermal stresses induced by deformation temperatures and rapid cooling with LN₂. Thus, at 600 °C, the thermal damage factors for (V_p) and (E) peaked by 85% and 95%, respectively, matching the significant heat damage in the granodiorite microstructure (Figures 7d and 14b) resulting from the elevated temperature and the quick shock and LN₂.

4.5. Liquid Nitrogen Cooling Impact Analysis

By comparing the pertinent characteristics of samples cooled rapidly by liquid nitrogen and those cooled slowly by Gomah et al. [15], it is possible to assess the cracking impact of liquid nitrogen and better analyze the effect of cooling techniques on high-temperature granodiorite. Hence, this part explored the additional cracking effects of liquid nitrogen cooling on high-temperature granodiorite's physical and mechanical properties. The P-wave velocity, porosity, UCS, and elastic modulus of liquid nitrogen-cooled samples were compared with those cooled by air, as shown in Figures 17 and 18.

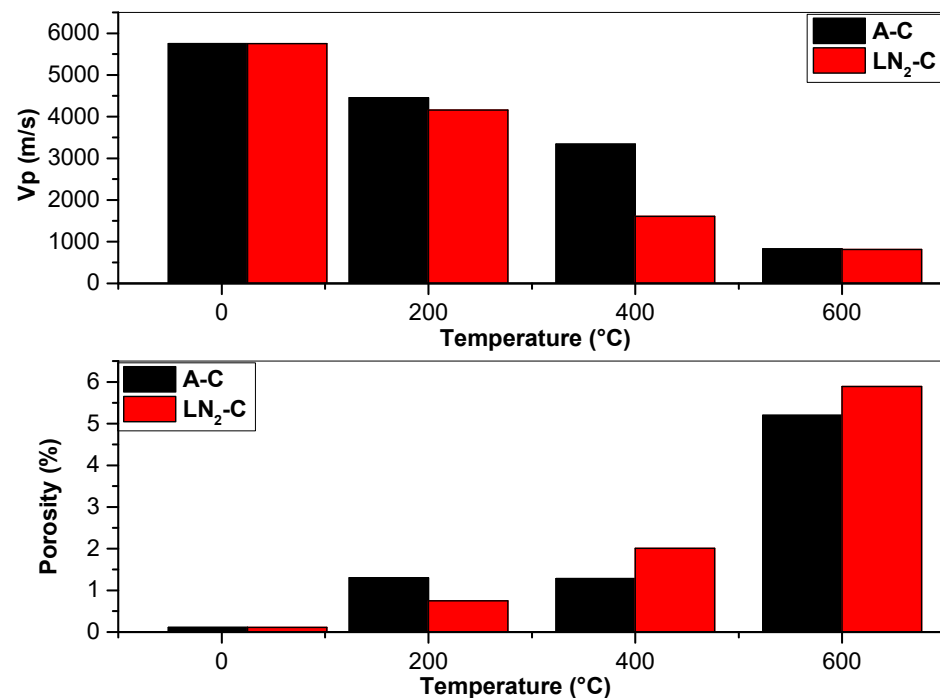


Figure 17. Cooling impact analysis on the physical properties of thermally heated granodiorite at various temperatures is followed by air cooling (A-C) and liquid nitrogen (LN₂).

As the heating temperature increased, the ultrasonic velocity of the specimens that were cooled naturally and those that were cooled using liquid nitrogen had a substantial declining tendency, as seen in Figure 17.

However, the specimen cooled with liquid nitrogen had a lower P-wave velocity than the sample cooled with air at the same temperature. This suggests that the damage from LN₂ cooling to the high-temperature granodiorite was higher. On the other hand, the porosity of the liquid nitrogen-cooled samples was lower than that of the air-cooled samples at 200 °C. However, the relationship swiftly shifted, demonstrating the effect of the LN₂ quench.

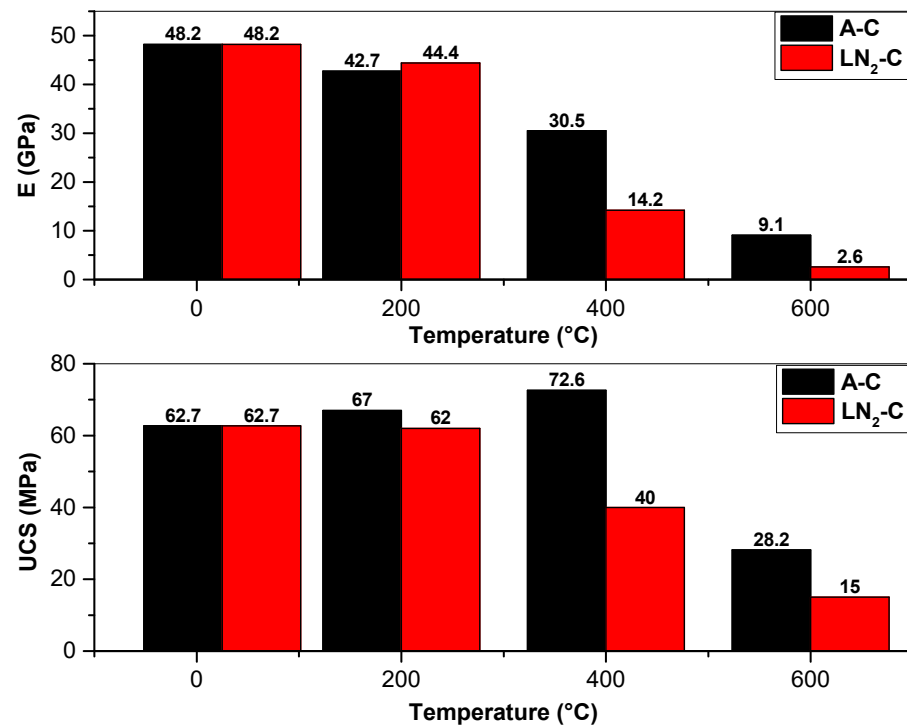


Figure 18. Cooling impact analysis on the mechanical properties of thermally heated granodiorite at various temperatures is followed by air cooling (A-C) and liquid nitrogen cooling (LN₂).

The samples cooled with liquid nitrogen showed a higher elastic modulus at 200 °C than those cooled with air, suggesting that the LN₂ quench had less effect at lower temperatures. However, the relationship abruptly changed beyond this temperature up to 600 °C, demonstrating the impact of quick quenching with LN₂. In contrast, the UCS of the liquid nitrogen-cooled specimen at the same temperature point was lower than that of the air-cooled sample, as illustrated in Figure 18.

Moreover, when the heating temperature was raised, the difference between the two samples rose and dropped afterward. The liquid nitrogen-cooled specimens had a higher cooling effect coefficient than the naturally cooled specimens, illustrating how the cooling impact of liquid nitrogen on granodiorite's properties starts to diminish as the temperature rises. LN₂ cooling causes more microcracks than A-C and significantly damages granodiorite samples. Therefore, compared to slow-cooling samples, the mechanical properties of samples that cool down quickly are exacerbated and diminished with temperature rise (Figure 18).

In summary, since liquid nitrogen can artificially create fractures in high-temperature rock, as demonstrated in Figure 17, it is possible to improve the stimulation efficiency of reservoirs in the extraction of nuclear and geothermal energy. Nevertheless, as Figure 18 shows, the propagation of initial fractures caused by hydraulic pressure and numerous subsequent fractures caused by LN₂ cooling can promote cooling-affected area expansion, which degrades the mechanical properties of granodiorite. Thus, to avoid or limit potential geological hazards, it is imperative to consider the possibility of a large-scale fracture net appearing inside the reservoir, which could decrease the mechanical characteristics of rocks while applying LN₂.

5. Conclusions

The behaviors of Egyptian granodiorite that underwent thermal treatment and LN₂ cooling were observed in this study using laboratory tests. Physical and mechanical parameters such as porosity, mass, volume, density, P-wave velocity, uniaxial compressive strength, and elastic modulus were investigated. X-ray diffraction, scanning electron mi-

croscopy, and optical microscopy also helped to observe the evolution of the microstructure. The principal conclusions are listed as follows:

- (1) Up to 300 °C, the porosity, crack density, thermal damage, and density reduction ratio progressively rose before drastically increasing beyond this point. Similarly, the uniaxial compressive strength climbed to 300 °C, and then it drastically dropped linearly as the temperature rose. In contrast, there was a gradual reduction in the elastic modulus and P-wave velocity as the temperature reached 200 °C, followed by a significant decline. Hence, this study revealed the following two mutation temperatures in the evolution of granodiorite mechanical and physical properties: 200 and 300 °C. After that, all metrics massively deteriorated;
- (2) Microcrack initiation and propagation can be associated with two primary granodiorite failure types. At 200 °C, tiny boundary and transgranular microcracks were visible, which led to the axial splitting modes. On the other hand, the shear failure mode was produced by developing boundary and transgranular cracks at 300, 400, and 600 °C;
- (3) Microscopically, the granodiorite exhibits boundary and transgranular cracks; however, boundary cracking is the main form of failure under thermal loading. Also, the impact of quartz on granodiorite thermal degradation is significant. Thus, most boundary cracks disperse at the quartz's borders. After being heated and cooled, granodiorite experiences many transgranular cracks at 600 °C; most occur in quartz;
- (4) Compared to air cooling, LN₂ cooling produces more notable changes in mechanical and physical characteristics, illustrating the cooling influence of liquid nitrogen on granodiorite's properties. Nevertheless, raising the desired heating temperature for both cooling methods causes more severe damage.
- (5) To avoid or reduce possible geological hazards, it is crucial to consider the adverse effects of using LN₂ for hydraulic fracturing stimulation, such as the weakening of host rocks' mechanical properties.

Subsequent research should concentrate on analyzing the environmental effects of various cooling techniques, specifically regarding water and energy consumption, to fulfill the urgent requirement for sustainable infrastructure development that places social welfare and environmental preservation at the forefront.

6. Recommendation

Future research may incorporate developing predictive models for estimating the extent of thermal damage in rocks based on heating and cooling parameters. Moreover, it will assess the effectiveness of various cooling rates in minimizing thermal cracking and preserving the rock's integrity, considering the environmental implications of different cooling strategies, particularly water usage and energy consumption.

Author Contributions: Conceptualization, M.E.G.; methodology, M.E.G. and A.A.O.; validation, M.E.G. and E.W.; analysis, M.E.G. and E.W.; lab tests, M.E.G. and A.A.O.; writing—original draft, M.E.G.; review and editing, M.E.G., E.W. and A.A.O.; supervision, E.W. All authors have read and agreed to the published version of the manuscript.

Funding: This research was funded by the National Natural Science Foundation of China (51934007).

Institutional Review Board Statement: Not applicable.

Informed Consent Statement: Not applicable.

Data Availability Statement: Data is contained within the article.

Conflicts of Interest: The authors declare no conflicts of interest.

References

1. Gallup, D.L. Production Engineering in Geothermal Technology: A Review. *Geothermics* **2009**, *38*, 326–334. [[CrossRef](#)]
2. Breede, K.; Dzebisashvili, K.; Liu, X.; Falcone, G. A Systematic Review of Enhanced (or Engineered) Geothermal Systems: Past, Present and Future. *Geotherm. Energy* **2013**, *1*, 4. [[CrossRef](#)]

3. Zhang, F.; Zhao, J.; Hu, D.; Skoczylas, F.; Shao, J. Laboratory Investigation on Physical and Mechanical Properties of Granite after Heating and Water-Cooling Treatment. *Rock Mech. Rock Eng.* **2018**, *51*, 677–694. [[CrossRef](#)]
4. Chen, Z.; Sha, S.; Xu, L.; Quan, J.; Rong, G.; Jiang, M. Damage Evaluation and Statistic Constitutive Model of High-Temperature Granites Subjected to Liquid Nitrogen Cold Shock. *Rock Mech. Rock Eng.* **2022**, *55*, 2299–2321. [[CrossRef](#)]
5. Feng, Z.; Zhao, Y.; Zhou, A.; Zhang, N. Development Program of Hot Dry Rock Geothermal Resource in the Yangbajing Basin of China. *Renew. Energy* **2012**, *39*, 490–495. [[CrossRef](#)]
6. Zhao, Y.; Feng, Z.; Xi, B.; Wan, Z.; Yang, D.; Liang, W. Deformation and Instability Failure of Borehole at High Temperature and High Pressure in Hot Dry Rock Exploitation. *Renew. Energy* **2015**, *77*, 159–165. [[CrossRef](#)]
7. Brook, B.W.; Alonso, A.; Meneley, D.A.; Misak, J.; Bles, T.; van Erp, J.B. Why Nuclear Energy Is Sustainable and Has to Be Part of the Energy Mix. *Sustain. Mater. Technol.* **2014**, *1*, 8–16. [[CrossRef](#)]
8. Xi, Z.; Yun, L.; Li, X.Z.; Huang, Z.; Lin, J.; Hua, X. Effects of Thermal Treatment on the Macroscopic Physical Properties and Microstructure of Beishan Fine-Grained Granite. *Bull. Eng. Geol. Environ.* **2022**, *81*, 190.
9. Ferrero, A.M.; Marini, P. Experimental Studies on the Mechanical Behaviour of Two Thermal Cracked Marbles. *Rock Mech. Rock Eng.* **2001**, *34*, 57–66. [[CrossRef](#)]
10. Freire-Lista, D.M. Thermal Stress-Induced Microcracking in Building Granite. *Eng. Geol.* **2016**, *206*, 83–93. [[CrossRef](#)]
11. Zhang, R.R.; Jing, L.W.; Ma, Q.Y. Experimental Study on Thermal Damage and Energy Evolution of Sandstone after High Temperature Treatment. *Shock Vib.* **2018**, *2018*, 3845353. [[CrossRef](#)]
12. Yang, S.-Q.Q.; Xu, P.; Li, Y.-B.B.; Huang, Y.-H.H. Experimental Investigation on Triaxial Mechanical and Permeability Behavior of Sandstone after Exposure to Different High Temperature Treatments. *Geothermics* **2017**, *69*, 93–109. [[CrossRef](#)]
13. Ding, Q.L.; Ju, F.; Mao, X.B.; Ma, D.; Yu, B.Y.; Song, S.B. Experimental Investigation of the Mechanical Behavior in Unloading Conditions of Sandstone after High-Temperature Treatment. *Rock Mech. Rock Eng.* **2016**, *49*, 2641–2653. [[CrossRef](#)]
14. Tripathi, A.; Gupta, N.; Singh, A.K.; Mohanty, S.P.; Rai, N.; Pain, A. Effects of Elevated Temperatures on the Microstructural, Physico-Mechanical and Elastic Properties of Barakar Sandstone: A Study from One of the World's Largest Underground Coalmine Fire Region, Jharia, India. *Rock Mech. Rock Eng.* **2021**, *54*, 1293–1314. [[CrossRef](#)]
15. Gomah, M.E.; Li, G.; Sun, C.; Xu, J.; Yang, S.; Li, J. On the Physical and Mechanical Responses of Egyptian Granodiorite after High-Temperature Treatments. *Sustainability* **2022**, *14*, 4632. [[CrossRef](#)]
16. Gomah, M.E.; Li, G.; Khan, N.M.; Sun, C.; Xu, J.; Omar, A.A.; Mousa, B.G.; Abdelhamid, M.M.A.; Zaki, M.M. Prediction of Strength Parameters of Thermally Treated Egyptian Granodiorite Using Multivariate Statistics and Machine Learning Techniques. *Mathematics* **2022**, *10*, 4523. [[CrossRef](#)]
17. Gomah, M.E.; Li, G.; Omar, A.A.; Abdel Latif, M.L.; Sun, C.; Xu, J. Thermal-Induced Microstructure Deterioration of Egyptian Granodiorite and Associated Physico-Mechanical Responses. *Materials* **2024**, *17*, 1305. [[CrossRef](#)] [[PubMed](#)]
18. Balme, M.R.; Rocchi, V.; Jones, C.; Sammonds, P.R.; Meredith, P.G.; Boon, S. Fracture Toughness Measurements on Igneous Rocks Using a High-Pressure, High-Temperature Rock Fracture Mechanics Cell. *J. Volcanol. Geotherm. Res.* **2004**, *132*, 159–172. [[CrossRef](#)]
19. Yang, T.; Sun, Q.; Dong, Z.; Ge, Z.; Wang, S.; Xu, C. A Study on Thermal Damage Mechanism of Sandstone Based on Thermal Reaction Kinetics. *Geomech. Geophys. Geo-Energy Geo-Resour.* **2021**, *7*, 64. [[CrossRef](#)]
20. Sundberg, J.; Back, P.-E.; Christiansson, R.; Hökmark, H.; Ländell, M.; Wrafter, J. Modelling of Thermal Rock Mass Properties at the Potential Sites of a Swedish Nuclear Waste Repository. *Int. J. Rock Mech. Min. Sci.* **2009**, *46*, 1042–1054. [[CrossRef](#)]
21. Feng, G.; Wang, X.; Wang, M.; Kang, Y. Experimental Investigation of Thermal Cycling Effect on Fracture Characteristics of Granite in a Geothermal-Energy Reservoir. *Eng. Fract. Mech.* **2020**, *235*, 107180. [[CrossRef](#)]
22. Zhou, L.; Zhu, Z.; Oterkus, E.; Oterkus, S.; Xu, H. Geohazard Mechanics Research on the Effects of Heating and Cooling Processes on the Mechanical Properties of Yellow Rust Granite. *Geohazard Mech.* **2023**, *1*, 231–243. [[CrossRef](#)]
23. Hou, P.; Liang, X.; Zhang, Y.; He, J.; Gao, F.; Liu, J. 3D Multi-Scale Reconstruction of Fractured Shale and Influence of Fracture Morphology on Shale Gas Flow. *Nat. Resour. Res.* **2021**, *30*, 2463–2481. [[CrossRef](#)]
24. Riahi, A.; Pettitt, W.; Damjanac, B.; Varun; Blanksma, D. Numerical Modeling of Discrete Fractures in a Field-Scale FORGE EGS Reservoir. *Rock Mech. Rock Eng.* **2019**, *52*, 5245–5258. [[CrossRef](#)]
25. Cheng, Y.; Zhang, Y.; Yu, Z.; Hu, Z. Investigation on Reservoir Stimulation Characteristics in Hot Dry Rock Geothermal Formations of China during Hydraulic Fracturing. *Rock Mech. Rock Eng.* **2021**, *54*, 3817–3845. [[CrossRef](#)]
26. King, G.E. Hydraulic Fracturing 101: What Every Representative, Environmentalist, Regulator, Reporter, Investor, University Researcher, Neighbor and Engineer Should Know about Estimating Frac Risk and Improving Frac Performance in Unconventional Gas and Oil Wells. In Proceedings of the SPE Hydraulic Fracturing Technology Conference and Exhibition, The Woodlands, TX, USA, 6–8 February 2012; SPE: Kuala Lumpur, Malaysia, 2012; p. SPE-152596.
27. Aguilera, R.F.; Ripple, R.D.; Aguilera, R. Link between Endowments, Economics and Environment in Conventional and Unconventional Gas Reservoirs. *Fuel* **2014**, *126*, 224–238. [[CrossRef](#)]
28. Cai, C.; Li, G.; Huang, Z.; Tian, S.; Shen, Z.; Fu, X. Experiment of Coal Damage Due to Super-Cooling with Liquid Nitrogen. *J. Nat. Gas Sci. Eng.* **2015**, *22*, 42–48. [[CrossRef](#)]
29. Zhou, Z.; Cai, X.; Li, X.; Cao, W.; Du, X. Dynamic Response and Energy Evolution of Sandstone under Coupled Static–Dynamic Compression: Insights from Experimental Study into Deep Rock Engineering Applications. *Rock Mech. Rock Eng.* **2020**, *53*, 1305–1331. [[CrossRef](#)]

30. Kumari, W.G.P.; Ranjith, P.G.; Perera, M.S.A.; Chen, B.K. Experimental Investigation of Quenching Effect on Mechanical, Microstructural and Flow Characteristics of Reservoir Rocks: Thermal Stimulation Method for Geothermal Energy Extraction. *J. Pet. Sci. Eng.* **2018**, *162*, 419–433. [[CrossRef](#)]
31. Kumari, W.G.P.; Ranjith, P.G.; Perera, M.S.A.; Chen, B.K.; Abdulagatov, I.M. Temperature-Dependent Mechanical Behaviour of Australian Strathbogie Granite with Different Cooling Treatments. *Eng. Geol.* **2017**, *229*, 31–44. [[CrossRef](#)]
32. Shao, S.; Wasantha, P.L.P.; Ranjith, P.G.; Chen, B.K. Effect of Cooling Rate on the Mechanical Behavior of Heated Strathbogie Granite with Different Grain Sizes. *Int. J. Rock Mech. Min. Sci.* **2014**, *70*, 381–387. [[CrossRef](#)]
33. Hou, P.; Gao, F.; Gao, Y.; Yang, Y.; Cai, C. Changes in Breakdown Pressure and Fracture Morphology of Sandstone Induced by Nitrogen Gas Fracturing with Different Pore Pressure Distributions. *Int. J. Rock Mech. Min. Sci.* **2018**, *109*, 84–90. [[CrossRef](#)]
34. Liang, X.; Hou, P.; Xue, Y.; Yang, X.; Gao, F.; Liu, J. A Fractal Perspective on Fracture Initiation and Propagation of Reservoir Rocks under Water and Nitrogen Fracturing. *Fractals* **2021**, *29*, 2150189. [[CrossRef](#)]
35. Hou, P.; Xue, Y.; Gao, F.; Dou, F.; Su, S.; Cai, C.; Zhu, C. Effect of Liquid Nitrogen Cooling on Mechanical Characteristics and Fracture Morphology of Layer Coal under Brazilian Splitting Test. *Int. J. Rock Mech. Min. Sci.* **2022**, *151*, 105026. [[CrossRef](#)]
36. Wu, X.; Huang, Z.; Song, H.; Zhang, S.; Cheng, Z.; Li, R.; Wen, H.; Huang, P.; Dai, X. Variations of Physical and Mechanical Properties of Heated Granite after Rapid Cooling with Liquid Nitrogen. *Rock Mech. Rock Eng.* **2019**, *52*, 2123–2139. [[CrossRef](#)]
37. Li, Q.; Yin, T.; Li, X.; Zhang, S. Effects of Rapid Cooling Treatment on Heated Sandstone: A Comparison between Water and Liquid Nitrogen Cooling. *Bull. Eng. Geol. Environ.* **2020**, *79*, 313–327. [[CrossRef](#)]
38. Kim, K.; Kemeny, J.; Nickerson, M. Effect of Rapid Thermal Cooling on Mechanical Rock Properties. In Proceedings of the Rock Mechanics and Rock Engineering, Vigo, Spain, 26–28 May 2014; American Rock Mechanics Association: Alexandria, VA, USA, 2014; Volume 47, pp. 2005–2019.
39. Zhang, H.; Huang, Z.; Zhang, S.; Yang, Z.; McLennan, J.D. Improving Heat Extraction Performance of an Enhanced Geothermal System Utilizing Cryogenic Fracturing. *Geothermics* **2020**, *85*, 101816. [[CrossRef](#)]
40. Yang, R.; Huang, Z.; Shi, Y.; Yang, Z.; Huang, P. Laboratory Investigation on Cryogenic Fracturing of Hot Dry Rock under Triaxial-Confining Stresses. *Geothermics* **2019**, *79*, 46–60. [[CrossRef](#)]
41. Shao, Z.; Wang, Y.; Tang, X. The Influences of Heating and Uniaxial Loading on Granite Subjected to Liquid Nitrogen Cooling. *Eng. Geol.* **2020**, *271*, 105614. [[CrossRef](#)]
42. Su, S.; Hou, P.; Gao, F.; Liang, X.; Ding, R.; Cai, C. Changes in Mechanical Properties and Fracture Behaviors of Heated Marble Subjected to Liquid Nitrogen Cooling. *Eng. Fract. Mech.* **2022**, *261*, 108256. [[CrossRef](#)]
43. Qin, L.; Zhai, C.; Liu, S.; Xu, J. Factors Controlling the Mechanical Properties Degradation and Permeability of Coal Subjected to Liquid Nitrogen Freeze-Thaw. *Sci. Rep.* **2017**, *7*, 3675. [[CrossRef](#)] [[PubMed](#)]
44. Read, H.; Hegemier, G.A. Strain Softening of Rock, Soil and Concrete—A Review Article. *Mech. Mater.* **1984**, *3*, 271–294. [[CrossRef](#)]
45. Zhang, W.; Sun, Q.; Hao, S.; Geng, J.; Lv, C. Experimental Study on the Variation of Physical and Mechanical Properties of Rock after High Temperature Treatment. *Appl. Therm. Eng.* **2016**, *98*, 1297–1304. [[CrossRef](#)]
46. Wu, X.; Huang, Z.; Li, R.; Zhang, S.; Wen, H.; Huang, P.; Dai, X.; Zhang, C. Investigation on the Damage of High-Temperature Shale Subjected to Liquid Nitrogen Cooling. *J. Nat. Gas Sci. Eng.* **2018**, *57*, 284–294. [[CrossRef](#)]
47. Huang, Z.; Wen, H.; Wu, X.; Li, G.; Yang, R.; Li, R.; Zhang, C. Experimental Study on Cracking of High Temperature Granite Using Liquid Nitrogen. *Zhongguo Shiyou Daxue Xuebao (Ziran Kexue Ban)* **2019**, *43*, 68–76.
48. Wu, X.; Huang, Z.; Cheng, Z.; Zhang, S.; Song, H.; Zhao, X. Effects of Cyclic Heating and LN₂-Cooling on the Physical and Mechanical Properties of Granite. *Appl. Therm. Eng.* **2019**, *156*, 99–110. [[CrossRef](#)]
49. Cha, M.; Alqahtani, N.B.; Yao, B.; Yin, X.; Kneafsey, T.J.; Wang, L.; Wu, Y.-S.; Miskimins, J.L. Cryogenic Fracturing of Wellbores under True Triaxial-Confining Stresses: Experimental Investigation. *SPE J.* **2018**, *23*, 1271–1289. [[CrossRef](#)]
50. El-Taher, A.; Uosif, M.A.M.; Orabi, A.A. Natural Radioactivity Levels and Radiation Hazard Indices in Granite from Aswan to Wadi El-Allaqi Southeastern Desert, Egypt. *Radiat. Prot. Dosim.* **2007**, *124*, 148–154. [[CrossRef](#)]
51. Streckeisen, A. Classification and Nomenclature of Volcanic Rocks, Lamprophyres, Carbonatites, and Melilitic Rocks: Recommendations and Suggestions of the IUGS Subcommittee on the Systematics of Igneous Rocks. *Geology* **1979**, *7*, 331–335. [[CrossRef](#)]
52. *ASTM D7012-14e1*; Test Method for Compressive Strength and Elastic Moduli of Intact Rock Core Specimens under Varying States of Stress and Temperatures. ASTM: West Conshohocken, PA, USA, 2010; pp. 1–8.
53. El-Ramly, M.F.; Akaad, M.K. The Basement Complex in the Central Eastern Desert, between Latitudes 24 30' and 25 40'. *Geol. Surv. Cairo* **1960**, *8*, 35.
54. Sabatakakis, N.; Koukis, G.; Tsiambaos, G.; Papanakli, S. Index Properties and Strength Variation Controlled by Microstructure for Sedimentary Rocks. *Eng. Geol.* **2008**, *97*, 80–90. [[CrossRef](#)]
55. Wang, G.; Zhang, X.; Liu, X.; Gao, H.; An, R.; Yan, L. Engineering Geological Characterization of Micaceous Residual Soils Considering Effects of Mica Content and Particle Breakage. *Eng. Geol.* **2023**, *327*, 107367. [[CrossRef](#)]
56. Nasser, M.H.B.; Tatone, B.S.A.; Grasselli, G.; Young, R.P. Fracture Toughness and Fracture Roughness Interrelationship in Thermally Treated Westerly Granite. *Pure Appl. Geophys.* **2009**, *166*, 801–822. [[CrossRef](#)]
57. Chaki, S.; Takarli, M.; Agbodjan, W.P. Influence of Thermal Damage on Physical Properties of a Granite Rock: Porosity, Permeability and Ultrasonic Wave Evolutions. *Constr. Build. Mater.* **2008**, *22*, 1456–1461. [[CrossRef](#)]

58. Gomah, M.E.; Li, G.; Xu, J.; Omar, A.A.; Haoran, H.; Zaki, M.M. Micro to Macro-Cracking Mechanism in Thermally Treated Granodiorite Followed by Different Cooling Techniques. *Int. J. Fract.* **2023**, *9*, 161–180. [[CrossRef](#)]
59. Sun, Q.; Zhang, W.; Qian, H. Effects of High Temperature Thermal Treatment on the Physical Properties of Clay. *Environ. Earth Sci.* **2016**, *75*, 610. [[CrossRef](#)]
60. Clark, S.P., Jr. *Handbook of Physical Constants*; Geological Society of America: Boulder, CO, USA, 1966; Volume 97.
61. Sun, Q.; Zhang, W.; Xue, L.; Zhang, Z.; Su, T. Thermal Damage Pattern and Thresholds of Granite. *Environ. Earth Sci.* **2015**, *74*, 2341–2349. [[CrossRef](#)]
62. Gomah, M.E.; Li, G.; Sun, C.; Xu, J.; Sen, Y.; Li, J.; Ismael, M.; Elkarmoty, M. Macroscopic and Microscopic Research on Egyptian Granodiorite Behavior Exposed to the Various Heating and Cooling Strategies. *Geomech. Geophys. Geo-Energy Geo-Resour.* **2022**, *8*, 1–22. [[CrossRef](#)]
63. Gomah, M.E.; Li, G.; Bader, S.; Elkarmoty, M.; Ismael, M. Damage Evolution of Granodiorite after Heating and Cooling Treatments. *Minerals* **2021**, *11*, 779. [[CrossRef](#)]
64. Shen, Y.J.; Hou, X.; Yuan, J.Q.; Wang, S.F.; Zhao, C.H. Thermal Cracking Characteristics of High-Temperature Granite Suffering from Different Cooling Shocks. *Int. J. Fract.* **2020**, *225*, 153–168. [[CrossRef](#)]
65. Rao, G.M.N.; Murthy, C.R.L. Dual Role of Microcracks: Toughening and Degradation. *Can. Geotech. J.* **2001**, *38*, 427–440. [[CrossRef](#)]
66. Zhao, H.B.; Yin, G.Z.; Chen, L.J. Experimental Study on Effect of Temperature on Sandstone Damage. *Chin. J. Rock Mech. Eng.* **2009**, *28*, 2784–2788.

Disclaimer/Publisher’s Note: The statements, opinions and data contained in all publications are solely those of the individual author(s) and contributor(s) and not of MDPI and/or the editor(s). MDPI and/or the editor(s) disclaim responsibility for any injury to people or property resulting from any ideas, methods, instructions or products referred to in the content.